

# LegoFormer: Transformers for Block-by-Block Multi-view 3D Reconstruction

Farid Yagubbayli<sup>1</sup>

farid.yagubbayli@tum.de

Yida Wang<sup>1</sup>

yida.wang@tum.de

Alessio Tonioni<sup>2</sup>

alessiot@google.com

Federico Tombari<sup>1,2</sup>

tombari@in.tum.de

<sup>1</sup>Technical University of Munich <sup>2</sup>Google Inc.

## Abstract

Most modern deep learning-based multi-view 3D reconstruction techniques use RNNs or fusion modules to combine information from multiple images after independently encoding them. These two separate steps have loose connections and do not allow easy information sharing among views. We propose *LegoFormer*, a transformer model for voxel-based 3D reconstruction that uses the attention layers to share information among views during all computational stages. Moreover, instead of predicting each voxel independently, we propose to parametrize the output with a series of low-rank decomposition factors. This reformulation allows the prediction of an object as a set of independent regular structures then aggregated to obtain the final reconstruction. Experiments conducted on *ShapeNet* demonstrate the competitive performance of our model with respect to the state of the art while having increased interpretability thanks to the self-attention layers. We also show promising generalization results to real data.

## 1. Introduction

Efficient, accurate, and interaction-less multi-view 3D reconstruction methods are a prerequisite for robotic perception, 3D object modeling and augmented reality applications. Structure-from-Motion (SfM) [30] and Simultaneous Localization and Mapping (SLAM) [13] provide viable solutions, however, they either fail or generate only partial shapes when only a set of non-overlapping views are available due to the inability to find correspondences among them. At the same time, this frequently occurs for practical applications: e.g., in 3D object modeling for online shopping only a small number of images from uncalibrated cameras are usually available.

Recently, several CNN-based techniques were proposed to overcome these limitations and reconstruct objects as a voxel grid from a few uncalibrated images with limited coverage. Methods like 3D-R2N2 [8] and LSM [19] treat multiple views as a sequence and utilize modified RNN models

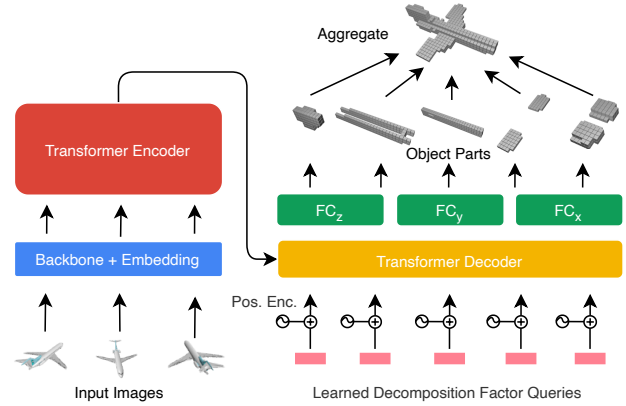


Figure 1. Given multiple views of an object, LegoFormer-M predicts a full 3D model as an aggregation of independently predicted parts. The subdivision of the 3D model into parts is obtained in a self-supervised way thanks to our problem formulation.

to fuse information from different views. RNNs, however, comes with drawbacks, such as long processing times, the difficulty of processing longer input sequences, and not being permutation invariant. More recent work [45, 46] proposed to replace the RNN model by first decoding each view separately into a full volume and then fusing them with independent fusion and refinement modules in the network. The modules need, however, to be trained progressively [45], making these solutions more complex to replicate. Lastly, all prior work predicts independently every voxel in the output 3D volume which can lead to non-regular reconstructions unless structural properties like smoothness and continuity are enforced explicitly.

To address these drawbacks, we propose *LegoFormer*: a model that uses a transformer network [40] to jointly encode all views and predict a 3D reconstruction in the form of its tensor decomposition. Fig. 1 illustrates a high-level overview of *LegoFormer*. We argue that transformers are particularly suited to the task at hand since their attention mechanism allows information sharing across the inputs token, i.e., the views in our case. This is in contrast with previ-

ous work based on CNNs and RNNs, where the knowledge from all views becomes available only once the encoding phase ends. For the special case of only one input view available, the attention mechanism would not provide any advantage. Therefore, we propose a special model for this task where patches from the same image are used as independent encoder inputs similarly to what is done in Vision Transformer (ViT) [10]. To differentiate between the two cases, the models are respectively named LegoFormer-M (multi-view) and LegoFormer-S (single-view).

For both models, we observe that most of the objects we want to reconstruct are man-made and therefore expected to have a certain regular structure. To leverage this property, we propose to use tensor decomposition to efficiently represent a voxel volume  $V \in \mathbb{R}^{N \times N \times N}$  by  $k$  decomposition factors of size  $\mathbf{d} \in \mathbb{R}^{3 \times N}$ . The decoder part of our architecture takes a set of learned encoded queries as input and transforms each one into three vectors (the decomposition factors). Taking a cross-product between each triplet of vectors gives a rank-1 estimation of the full output voxel grid. We show how different queries generate different estimations corresponding to individual parts of the object, e.g., the body of a plane or the wings in Fig. 1; combining the parts together provides then the full model. Remarkably, we do not provide explicit supervision for the different parts but let the network figure out a good subdivision as it is the only way of minimizing the loss functions given the constraints on the output space.

We evaluate our proposal on ShapeNet [5], showing competitive performance against prior techniques with more regular predictions and improved interpretability. We also test the generalization of our method on real images from Pix3D [36]. To summarize our contributions:

- i) we introduce LegoFormer, a novel architecture for single- and multi-view object reconstruction that uses self-attention for both jointly encoding the input views and predicting the output volume;
- ii) we propose to parametrize the output grid by its decomposition factors to take advantage of the inherent structures in common objects, and reformulate the task as the prediction of these factors;
- iii) we show how LegoFormer learns to decompose a shape into a sum of tensor decomposition factors without explicit supervision for it.

## 2. Previous work

**3D Reconstruction:** Classic techniques like SfM [30] and SLAM [13] rely on feature extraction and matching across different views. Both steps assume highly overlapping views and Lambertian surfaces that limit their use. With the availability of large 3D object datasets and advances in deep learning, a new category of learned methods emerged. The majority of techniques for multi-view 3D

reconstruction [8, 19, 45, 46] use an encoder-decoder architecture to map 2D images into 3D volumes without using 3D surfaces as intermediate representation. The mapping is done individually on each image therefore discarding information shared among views. Methods like 3D-R2N2 [8] and LSM [19] introduce recurrent models to combine information from individual 3D volumes into a single volume, while Pix2Vox [45, 46] uses a dedicated fusion unit. [35] regresses the view poses and uses silhouettes to build an initial volume, then, as also done in LSM and Pix2Vox, uses a refiner unit that makes corrections to the predicted volumes based on the shape priors acquired during training. In contrast to these works, LegoFormer combines encoding, fusion, and decoding under a single transformer model. This structure allows the use of information from all the views in every stage of the process, resulting in a more tightly integrated framework.

**Transformers:** Transformers have shown enormous success in a large variety of NLP tasks since their introduction by [40]. Recent work started to utilize transformer models for computer vision tasks by reformulating the inputs, which are mostly 2D RGB images, as a sequence of tokens [2, 4, 10]. ViT [10] is one of the earliest image classification methods that use a transformer encoder directly on a sequence of image patches. DETR [4] combines a pre-trained CNN backbone with an encoder-decoder transformer and predicts a sequence of bounding boxes in parallel. TimeSformer [2] has extended ViT with a spatiotemporal attention mechanism and achieves higher performance with less training time in video understanding tasks. More recently, hybrid approaches like LeViT [14] emerged where the convolutional blocks are integrated into the transformer model. Concurrently to our work [42] explored the use of a transformer-based model for 3D object reconstruction. Although there are similarities between the two works, our decoding scheme is significantly different. To the best of our knowledge, together with [42] we are the first works to explore the use of transformer-based models for 3D shape reconstruction from multiple-views.

**Compressed Representation:** An efficient representation is crucial when working with detailed 3D objects. Techniques like Distance Field Compression [18], Octree [48] and Voxel Hashing [29] exploit sparseness of the voxel volume and achieve 5-10 times compression rates [3]. These methods use specialized data structures that often require complex mapping to the original 3D volume. On the other hand, TT-TSDF [3] uses Low-Rank Tensor Train decomposition to represent the 3D tensor with lower rank tensors and demonstrates its application on the TSDF volumes. PARAFAC [16] and Tucker [23, 39] are alternative general purpose decomposition algorithms where the latter has higher stability [3]. Modified algorithms for boolean matrix decomposition were proposed by [33] and [41] by introduc-

ing constraints over the decomposition factors. Matrix factorization is also used widely in recommendation systems to understand relationships [21]. The LegoFormer output representation is similar to the one in PARAFAC with a modification that bounds the decomposition factors in the range  $[0, 1]$  to ensure binary decomposition. Negative numbers are not included in the prediction range to avoid "deletion" of the object parts during the aggregation phase.

### 3. Methodology

#### 3.1. LegoFormer

**Overview:** Fig. 1 provides an overview of the proposed architecture. LegoFormer uses a vanilla pre-norm encoder/decoder transformer model [28] to reconstruct a 3D occupancy grid of size  $32^3$  from a set of 2D views. Each view is first mapped to an input token by a CNN-backbone. On the encoder side, the inputs are jointly encoded using the self-attention mechanism. Then the encoded inputs are passed to a non-autoregressive decoder together with a set of learned input queries. The decoder processes each query into a  $32^3$  volume containing a "part" of the full object. Each "part" volume is parametrized by three vectors and calculated as the outer product between them. The final occupancy grid is the sum of the predicted parts. We do not supervise the subdivision of the objects into parts during training, which emerges naturally, instead, thanks to the architecture and the constrained output space. Considering a single-view reconstruction, the attention mechanism on the encoder side would not do anything with the formulation described so far. For this reason, we also propose a variant of our method tailored for the single view case, where the input tokens are obtained from the patches of a single view instead of the full image. We will refer to the two variants of our method as LegoFormer-M and LegoFormer-S for the multi- and single-view cases to differentiate between the two scenarios, respectively.

**Backbone and Embedding:** Due to the high spatial dimensionality of the input 2D images ( $224 \times 224 \times 3$ ), it is not feasible to feed them directly into the transformer, which typically has a much lower dimensionality. We use a VGG16 [34], pre-trained on ImageNet [9], followed by  $c$  additional convolutional layers to map images to a compact feature representation  $\psi$ , as in [4, 46]. Each convolutional layer is followed by batch normalization and a ReLU activation. The VGG16 is frozen during training while the convolutional layers are trained.

*LegoFormer-M:* uses  $c = 3$  convolution blocks with a MaxPool after the second block with kernel size 2. The output features have size  $\psi = 8 \times 8 \times 64$  and are flattened and then projected using a single fully connected layer to obtain the input tokens for the transformer model.

*LegoFormer-S:* uses  $c = 1$  convolution block that results

in an output size  $\psi = 28 \times 28 \times 48$ . The input sequence for LegoFormer-S is defined as a set of square patches of size  $p = 4$  extracted from  $\psi$  resulting in  $\frac{28}{4} \cdot \frac{28}{4} = 49$  input tokens. Each patch is projected using a single fully connected layer to obtain the input tokens for the transformer.

**Encoding:** We use a vanilla transformer encoder with pre-norm residual connections [28] to encode the input tokens. Each input token is allowed to attend to any other input while being encoded, so no self-attention mask is used. The pre-norm residual connections are preferred over post-norm connections due to the increased training stability. We do not use any positional encoding in LegoFormer-M to achieve input permutation invariance. Nevertheless, in LegoFormer-S we add to the input tokens a 2D positional sin-cos encoding [31] to inject the spatial relation between patches.

**Decoding:** The decoder also uses the vanilla pre-norm transformer [28] and a non-autoregressive formulation where the predictions are made in parallel. Following DETR [4] we use learned decoder inputs, denoted decomposition factor queries, as input at the first decoder layer. The queries of the same size as the transformer dimensionality are initialized from a normal distribution with  $\mu = 0$  and  $\sigma = 1$ . In contrast to the encoder, an attention mask is applied to prevent queries from attending to themselves. We experimentally found that such masking leads to a slight increase in performance compared to no masking. A 1D positional sin-cos encoding [31] is added to each learned query before passing it to the decoder. This addition is necessary to help distinguish between queries and avoid the collapse of all outputs to the same value during training.

**Output:** The raw decoder outputs  $Y_i$  are linearly projected using three fully connected layers  $FC_{\{z,y,x\}}$  into three vectors of size  $\mathbb{R}^{32}$  corresponding to the decomposition factor components. After applying a sigmoid activation  $\sigma$ , we use a cross-product ( $\otimes$ ) between the vectors to obtain a rank-1 estimation of the entire voxel grid. Each query is decoded into a rank-1 estimation, and all of them are combined by sum-aggregation to obtain the final reconstruction  $P$ . Formally, this is defined as

$$\mathbf{z}_i, \mathbf{y}_i, \mathbf{x}_i = FC_3(Y_i) \quad (1)$$

$$\mathbf{z}_i, \mathbf{y}_i, \mathbf{x}_i = \sigma(\mathbf{z}_i), \sigma(\mathbf{y}_i), \sigma(\mathbf{x}_i) \quad (2)$$

$$P = \min(1, \sum_i \mathbf{z}_i \otimes \mathbf{y}_i \otimes \mathbf{x}_i) \quad (3)$$

As the target values are in the range  $[0, 1]$  the sigmoid is a suitable activation function. We clip the aggregated volume to prevent voxels with values larger than 1 after the sum-aggregation. The clipping also replicates the rules of boolean algebra where  $1 + 1 = 1$  [27]

**Loss function:** We use Mean-Squared-Error as the loss function to train the network. It is calculated between the

predicted reconstruction and the ground-truth volume  $G$  as follows:

$$\mathcal{L}_{mse}(P, G) = \frac{1}{N^3} \sum_{i=0}^N \sum_{j=0}^N \sum_{k=0}^N (P_{i,j,k} - G_{i,j,k})^2 \quad (4)$$

### 3.2. Alternative Schemes

During the development of this work we explored several alternatives to the tensor decomposition-based schema for the decoder part of our network. The alternative approaches subdivide the output volume into fixed patches and predict each one explicitly. Three such schemes are described below. Note that they are not strictly related to the proposed LegoFormer but they might be relevant for practitioners in the field. We will show a comparison between all alternatives in Sec. 4.7.

**Naive:** A simple approach for the output sequence subdivides the output volume into an ordered list of 3D patches of size  $4^3$  and predicts them sequentially using a transformer decoder in an auto-regressive fashion. A causal mask [40] for the decoder-side attention is used during the training to prevent the decoder inputs from attending to future elements of the sequence. Formally,

$$Y_i = \mathcal{D}(\mathcal{E}, P_{0..i-1}) \quad (5)$$

$$P_i = \sigma(FC(Y_i)) \quad (6)$$

$$P = \text{reshape}(P_0, P_1, \dots, P_n) \quad (7)$$

Where  $\mathcal{D}$  and  $\mathcal{E}$  are the transformer decoder and the encoded views, respectively. Afterward, the predicted 3D patches are stitched together to obtain the total volume.

**Naive-nAR:** The above approach will result in low throughput performance during the inference due to the patches being predicted one by one. An alternative way, denoted "Naive-nAR", is predicting all patches simultaneously using a non-autoregressive decoder, which will significantly decrease the inference time. Formally,

$$P_i = \sigma(FC(\mathcal{D}(\mathcal{E}, \mathbf{l}_i))) \quad (8)$$

$$P = \text{reshape}(P_0, P_1, \dots, P_n) \quad (9)$$

where  $\mathbf{l}_i$  is a learned query as in the LegoFormer.

**Naive-Full:** Predicting the output volume in patches is computationally expensive and not scalable. Given a grid of side 32 and a patch of side 4, it will take  $8^3 = 512$  predictions to cover the whole volume. Although transformers can efficiently attend to long sequences, the memory requirement grows quadratically [1] with the output sequence length. In order to reduce the number of predictions required, the whole volume can be predicted at once using

a single learned query. However, this sacrifices the use of attention on the decoder. The scheme can be defined as,

$$P = \sigma(FC(\mathcal{D}(\mathcal{E}, \mathbf{l}))) \quad (10)$$

## 4. Experiments

### 4.1. Evaluation protocol and implementation details

**Dataset:** Following [8, 45, 46] we use rendered images from ShapeNet [44] to evaluate the proposed method. To have comparable results, we follow the settings of [8] and use a subset of ShapeNet, which includes 43783 models from 13 categories. Each model is rendered from 24 different poses. The original images of size  $137 \times 137$  are resized to  $224 \times 224$  and a uniform background color is applied before passing them to the network. The ground truth targets are 3D occupancy grids with size  $32^3$  and target volumes aligned to a canonical reference frame.

**Metrics:** 3D Intersection over Union (IoU) and F-score are used to measure the reconstruction performance. Given predicted  $\mathcal{R}$  and ground-truth  $\mathcal{G}$  occupancy volumes, the former measures the ratio of intersecting voxels from both volumes to their union. The ratio ensures that the calculation is object size independent. The latter metric, proposed by [20], focuses on the quality of the surface reconstruction and measures the percentage of points from the object surfaces that are closer than a predefined threshold. We follow the setup of [46] to convert the predicted volumes to point clouds and use the implementation provided by [38] for calculating the F-score. For both metrics, a higher value means better reconstruction.

**Implementation Details:** Both LegoFormer-M and LegoFormer-S are trained with batch size 128 using  $224 \times 224$  RGB images as input and  $32^3$  voxelized reconstructions as output. The models are implemented using PyTorch-Lightning [12] and trained on Nvidia A100 and T4 GPUs on Google Cloud Platform (GCP) using Adagrad optimizer [11]. The learning rate is set to 0.01 with 10K warmup steps. For multi-view models, the number of input views is fixed to 8 during the training as we experimentally found that fixing the view count helps to achieve higher performance than updating it between steps (experiments reported in the Supplementary Sec. A.2). The views are randomly sampled out of 24 views at each iteration. The number of layers for both encoder and decoder is set to 8. The transformer dimensionality is set to 768 and 4096 for input token and feed-forward layer, respectively. After running ablation studies with different number of decoder queries, the decoder input count is fixed to 12, meaning that the reconstructed volume is formed from 12 rank-1 estimations. At inference time after the sum-aggregation and clipping, we use a threshold  $\tau = 0.3$  to obtain the occupancy grid.



Model	Number of Views								
	1	2	3	4	5	8	12	16	20
<b>Metric: IoU</b>									
3D-R2N2 [8]	0.560	0.603	0.617	0.625	0.634	0.635	0.636	0.636	0.636
AttSets [47]	0.642	0.662	0.67	0.675	0.677	0.685	0.688	0.692	0.693
Pix2Vox/F [45]	0.634	0.660	0.668	0.673	0.676	0.680	0.682	0.684	0.684
Pix2Vox/A [45]	0.661	0.686	0.693	0.697	0.699	0.702	0.704	0.705	0.706
Pix2Vox++/F [46]	0.645	0.669	0.678	0.682	0.685	0.690	0.692	0.693	0.694
Pix2Vox++/A [46]	<b>0.670</b>	<b>0.695</b>	<b>0.704</b>	<b>0.708</b>	<b>0.711</b>	<b>0.715</b>	<b>0.717</b>	<b>0.718</b>	<b>0.719</b>
LegoFormer-M	0.519	0.644	0.679	0.694	0.703	0.713	<b>0.717</b>	<b>0.719</b>	<b>0.721</b>
LegoFormer-S	0.655	-	-	-	-	-	-	-	-
<b>Metric: F-score @ 1%</b>									
3D-R2N2 [8]	0.351	0.368	0.372	0.378	0.382	0.383	0.382	0.382	0.383
AttSets [47]	0.395	0.418	0.426	0.430	0.432	0.444	0.445	0.447	0.448
Pix2Vox/F [45]	0.364	0.393	0.404	0.409	0.412	0.417	0.420	0.423	0.423
Pix2Vox/A [45]	0.405	0.435	0.448	0.449	0.452	0.456	0.458	0.459	0.460
Pix2Vox++/F [46]	0.394	0.422	0.432	0.437	0.440	0.446	0.449	0.450	0.451
Pix2Vox++/A [46]	<b>0.436</b>	<b>0.452</b>	<b>0.455</b>	<b>0.457</b>	<b>0.458</b>	0.459	0.460	0.461	0.462
LegoFormer-M	0.282	0.392	0.428	0.444	0.453	<b>0.464</b>	<b>0.470</b>	<b>0.472</b>	<b>0.473</b>
LegoFormer-S	0.404	-	-	-	-	-	-	-	-

Table 1. Comparison of multi-view reconstruction between models on ShapeNet at  $32^3$  resolution. Mean IoU and F-Score@1% reported for all categories.

LegoFormer-M is trained for 80K steps, while LegoFormer-S is trained for 160K steps. No learning rate decay was used. Obtaining the reconstructed volumes from the decomposition factors is implemented using Einstein Summation for efficient use of the memory. We use data and implementations along with pre-trained models provided by authors under the MIT License for comparison to other works. Our code and trained models will be made publicly available.

## 4.2. Multi-view Reconstruction

We start by evaluating the multi-view reconstruction performance of LegoFormer-M against 3D-R2N2 [8], AttSets [47], Pix2Vox [45], and Pix2Vox++ [46]. As shown in Tab. 1 the proposed method slightly outperforms other techniques when more than 12 views are given. The difference in F-score is higher than the difference in IoU, meaning that LegoFormer reconstructs object surfaces better. The performance for a lower number of views is comparable to the state-of-the-art method Pix2Vox++ and the method outperforms 3D-R2N and AttSets when two or more views are given. Increasing the number of input views increases the performance of all methods, however for our method the gain is higher thanks to the use of the attention mechanism during the view encoding. For example, we get a +12.5 mIoU between not using encoder side attention (1 view) and using it (2 views), showing the impact of this component.

Fig. 2 displays examples of reconstructions obtained from 4 input views (only 3 are shown). In general, the reconstructions by LegoFormer tend to have less noise and smoother surfaces. This property can be attributed to the constraints that our tensor decomposition imposes. Since

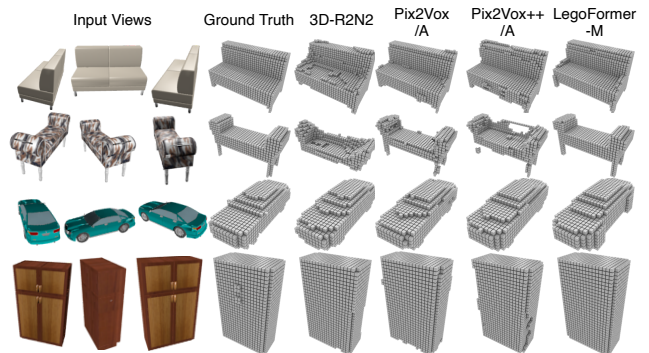


Figure 2. Multi-view object reconstructions for 4 input views (only 3 are shown) on ShapeNet with  $32^3$  resolution.

the output is an aggregation of rank-1 tensors obtained as the cross-product between three vectors, it is harder for the network to predict random spike-like voxels and non regular surfaces. This formulation naturally acts as a regularizer that forces to reconstruct the object from well-connected chunks. Qualitative examples of this are the sitting and the backrest areas of the bench and sofa reconstructions.

## 4.3. Comparison to Multi-view 3D Reconstruction with Transformer [42]

Concurrently with our work, Wang et al. [42] developed a similar model based on a transformer architecture for multi-view reconstruction. In [42], the encoder side of the transformer takes full views as input, as we do, but uses a different attention mechanism to foster different representations for each view. On the decoder side, instead, they stick

Model	Evaluation view count						
	4	6	8	12	16	20	24
<b>IoU</b>							
VoIT [42]	0.605	0.662	0.681	0.699	0.706	0.711	0.714
VoIT+ [42]	0.695	0.704	0.707	0.711	0.714	0.715	0.716
EVotT [42]	0.609	0.675	0.698	<b>0.720</b>	<b>0.729</b>	<b>0.735</b>	<b>0.738</b>
LegoFormer-M	<b>0.694</b>	<b>0.709</b>	<b>0.713</b>	0.717	0.719	0.721	0.721
<b>F-Score@1%</b>							
VoIT [42]	0.356	0.410	0.430	0.450	0.459	0.464	0.468
VoIT+ [42]	<b>0.451</b>	<b>0.460</b>	<b>0.464</b>	0.469	0.472	0.474	0.475
EVotT [42]	0.358	0.423	0.448	<b>0.475</b>	<b>0.486</b>	<b>0.492</b>	<b>0.497</b>
LegoFormer-M	0.444	<b>0.460</b>	<b>0.464</b>	0.470	0.472	0.473	0.474

Table 2. Comparison to the concurrent work by Wang et al. [42] including three variations of their proposed architecture.

to a more vanilla formulation and use a decoding schema similar to our Naive-nAR variant described in Sec. 3.2. Unfortunately, the authors of [42] did not release their code nor their trained models, making an extensive comparison challenging. We tried to replicate their results following the description on the paper, but unfortunately we were not able to achieve the good performance reported. As such we present here only a preliminary comparison between the two works, with the caveat of taking the performance for [42] directly from the paper. In Tab. 2 we compare three variants of the method proposed in [42] (rows 1,2,3) and our model. Our formulation is competitive or better than [42] for a low view count, while for an high view count we perform slightly worse than EVotT but better than the other variants. Among the three variants of [42] EVotT is the only one using an enhanced attention schema in the encoder part of the network, one of the main contributions of [42]. We believe that these experimental results show how our decoding schema is superior to the one used in [42] while their enhanced attention helps in the case of many views provided as input. Combining the strength of both methods is an exciting future development for this branch of works, however, as mentioned, replicating the result of EVotT has proven challenging. Finally, while [42] proposes models optimized for inference mainly on many input views, we preferred to develop methods with more consistent performance also on a low number of views, getting to the extreme of LegoFormer-S which is explicitly designed to achieve good performance with a single input view and which we are going to evaluate next.

#### 4.4. Single-view Reconstruction

The first column of Tab. 1 compares LegoFormer-S and LegoFormer-M against state-of-the-art methods for single-view object reconstruction. As expected LegoFormer-S, which uses image patches as input tokens, outperforms LegoFormer-M, which uses the full image as a single to-

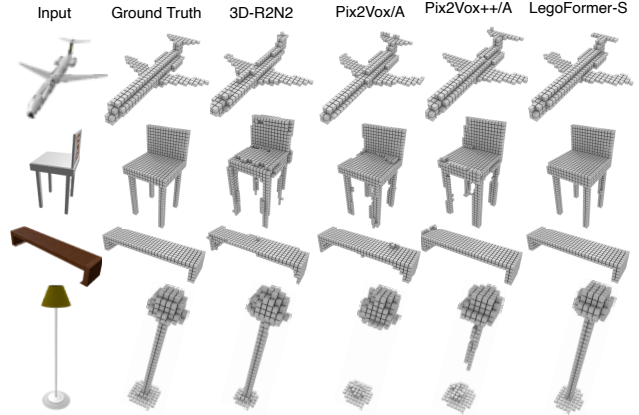


Figure 3. Single-view object reconstructions on ShapeNet with  $32^3$  resolution.



Figure 4. Reconstruction of real-world objects from Pix3D [36] obtained by a LegoFormer-S model trained only on ShapeNet [5]. The four leftmost samples represent categories present in ShapeNet, while the *Misc.* one is unknown to the model.

ken, showing again the advantage of using the attention mechanism on the encoder. LegoFormer-S shows superior performance with respect to all competitors except for Pix2Vox++/A. Some examples of single view reconstruction are shown in Fig. 3, highlighting how, once again, the shapes predicted by LegoFormer-S are much smoother and more regular than the one predicted by the competitors. A category-wise comparison to the other single-view reconstruction techniques is reported in the Supplementary Sec. B.

#### 4.5. Single-view reconstruction from real images

To test the generalization performance of our method, we test it on real-world settings using the Pix3D dataset [36]. Pix3D provides a single view for various real objects together with a segmentation masks. For each object we use the mask to segment out the background and replace it with a constant color. The resulting images are provided as input to a LegoFormer-S trained only on Shapenet and we report examples of the predicted models for different categories in Fig. 4. In particular the four leftmost samples represent

categories overlapping the ShapeNet ones, while the *Misc.* sample represent a completely unseen category. The quality of the reconstructions highlights how our method can successfully generalize across domains (synthetic-to-real) and, partially, also to completely unseen categories (*Misc.*). More results are reported in the supplementary material.

#### 4.6. Model Analysis

During the development of this work we found out that we can get insight on the reconstruction process of LegoFormer by analyzing and visualizing the attention scores. Our architecture uses 3 types of attention: encoder-to-encoder, decoder-to-encoder and decoder-to-decoder. The second gives information on where the network "looks" when reconstructing specific parts. The last identify which parts are taken into account when decoding a specific query.

Fig. 5 visualizes the attention scores for two examples from a LegoFormer model trained with 6 queries. We use a reduced number of queries for this experiment to ease the visualization. First, the network pays more attention to the airplane body while reconstructing its tail, likely because the tail can be predicted by looking at the plane's body. Second, when reconstructing a specific part, the surrounding parts get more attention, e.g., the last three columns of the airplane and the first two for the chair. Also, parts split in multiple pieces, like the airplane wings and chair backrest have significantly higher attention for the other adjacent pieces. Consistency could be an explanation for these observations, i.e., the network tries to make sure that predicted parts fit well together. Last but not least, one of the input views usually gets the majority of the attention from the decoder side. This suggests that the model is focusing on a single output of the encoder as "reference" to guide the reconstruction, while the others are mainly used to refine details. Indeed, thanks to the attention layers, each encoder outputs represent the corresponding input view, but also aggregates information coming from the others.

We also show the encoder-decoder attention for LegoFormer-s in Fig. 6. In LegoFormer-S the decoder attending to individual outputs of the encoder focuses on particular patches of the input view, therefore we opted for a heat-map to plot the attention. To enhance the visualization we trained a special version of LegoFormer-S using input patches of size  $1^2$ . The attention maps give insights into where the network "looks" when predicting a particular block. First, as expected, the attention is always higher on the object and surrounding parts, likely to understand the silhouette of the object. Second, the attention can be focused on a particular place or distributed over a larger area. For example, while predicting the tail of the plane (first and second row), the attention is spread all over the plane's body. In contrast, while reconstructing the chair legs (third row), it is very focused on that part only. The reason

Views	IoU				F-Score@1%			
	Naive	Naive-nAR	Naive-Full	LegoFormer-M	Naive	Naive-nAR	Naive-Full	LegoFormer-M
1	0.500	0.557	0.558	<b>0.617</b>	0.290	0.333	0.337	<b>0.364</b>
2	0.552	0.640	0.643	<b>0.674</b>	0.339	<b>0.427</b>	0.426	0.422
3	0.567	0.663	0.659	<b>0.689</b>	0.353	<b>0.456</b>	0.447	0.438
4	0.573	0.670	0.668	<b>0.695</b>	0.359	<b>0.464</b>	0.458	0.445
5	0.577	0.676	0.672	<b>0.699</b>	0.363	<b>0.472</b>	0.463	0.449
8	0.582	0.681	0.675	<b>0.704</b>	0.367	<b>0.480</b>	0.467	0.455
12	0.583	0.685	0.680	<b>0.706</b>	0.369	<b>0.486</b>	0.474	0.457
16	0.584	0.686	0.681	<b>0.707</b>	0.371	<b>0.489</b>	0.477	0.459
20	0.585	0.687	0.681	<b>0.708</b>	0.372	<b>0.489</b>	0.476	0.459

Table 3. Comparison of multi-view reconstruction performance of the decoding schemes on ShapeNet at  $32^3$  resolution. Mean IoU and F-Score@1% reported for all categories. All models are trained with 4 input views.

behind this difference could be that the shape of the plane tails have higher variance, and "looking" to other parts is helpful, while the chair legs are more or less similar to each other and self-sufficient for the reconstruction. Lastly, the decoder attends to similar parts of the images when reconstructing nearby blocks. For example, when reconstructing the central parts of the sitting of the chair (last two rows) the attention maps generated look quite similar, showing a strong relationship between the shape being generated and on which part of the input view the model decides to attend.

Finally, during our experiments we always observed intra- and inter- category consistency in how the queries get decoded into object parts. Fig. 7 displays incremental reconstructions obtained aggregating decoded queries for 2 categories each with 2 examples. For both tables, the first queries predict the bottom parts, while the last ones predict the top. A similar pattern exists for chairs - the backrest gets predicted by the first queries followed by the legs and the seat. Furthermore, we observe some form of consistency between categories: the first queries tend to predict the bottom and sides of the object while the lasts predict the top part and the inside. These experimental observations suggest that during the training, each query specialize on specific parts that are similar between objects from the same and different categories.

#### 4.7. Comparison to other decoding schemes

To experimentally validate our design choices we compare the four decoding schemes described in Sec. 3.2 in Tab. 3. All models are trained on 4 input views. LegoFormer achieves the highest IoU in all view counts while both "Naive-nAR" and "Naive-Full" have higher F-score performance suggesting that the former is better for objects

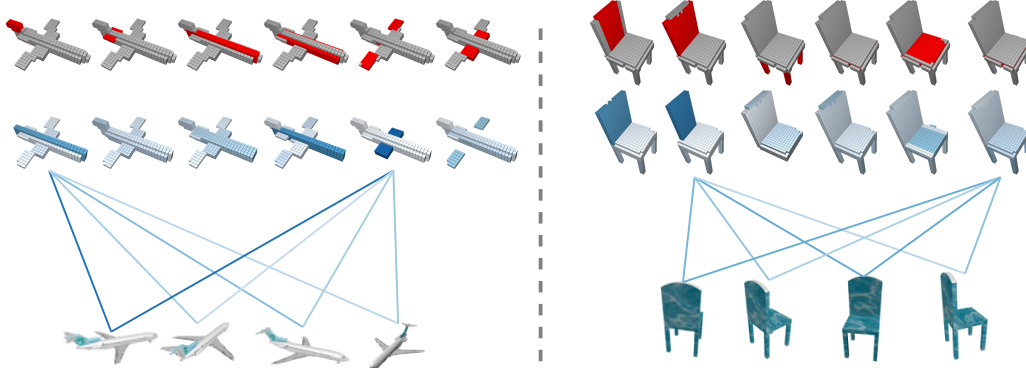


Figure 5. Visualization of the decoder-to-decoder (top) and decoder-to-encoder (bottom) attention for a LegoFormer-M model trained with 6 queries. Red color shows the part being reconstructed. Shades of blue denotes the attention score with darker meaning higher. The decoder-to-encoder attention is visualized for two queries for simplicity.

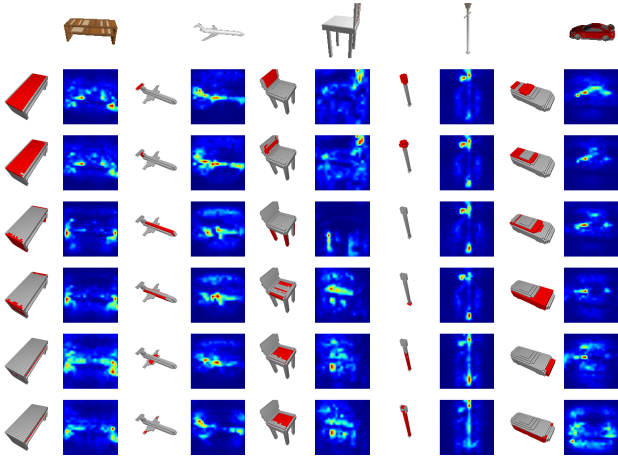


Figure 6. Decoder-to-Encoder attention for LegoFormer-S trained with input patch size  $1^2$ . The input image is shown in the top row, odd columns show the part being reconstructed by each query (in red), while even columns plot the attention on the input tokens with a jet color map.

with solid interior while the latter are good at reconstructing surfaces. The "Naive-nAR" decoding scheme constantly achieves the highest F-score except for a single view case. Compared to LegoFormer, it solves an easier task where the subspace predicted by each query is predefined and doesn't change. However, the memory requirement is much higher, making it a less attractive solution when considering scaling the output resolution. Finally, "Naive-Full" is the most canonical architecture directly predicting each voxel independently. This solution is still competitive but suffers from the same scalability problem of "Naive-nAR" when increasing the output resolution. The "Naive" model has the worst performance, which can be attributed to accumulated error. As the predictions are made in sequence while conditioning on previous steps, a slight mistake at some early steps will result in wrong predictions later on. We observed a huge

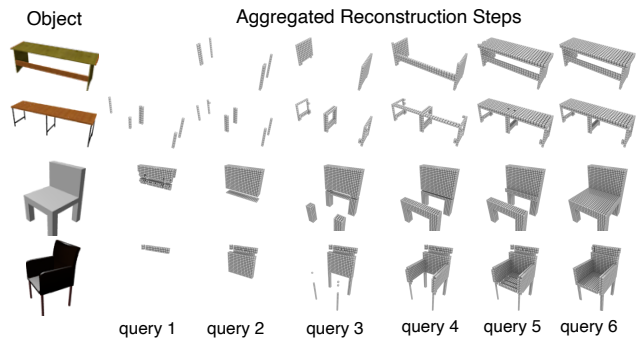


Figure 7. Reconstruction from a model trained with 6 queries on Shapenet. We show aggregated results for each query, i.e., the model above query 2 represent the output of query 1 + query 2.

gap between train and test performance for this model, leading us to conclude that autoregressive decoding schemes are not good candidates for 3D voxel grid reconstruction. An additional qualitative comparison of the decoding schemes is provided in the Supplementary Sec. C.

## 5. Conclusion & Discussion

We presented LegoFormer, a transformer model to reconstruct an object from multiple views via its decomposition factors. In contrast to previous works, the proposed method combines view encoding and volume prediction under the same network and allows information sharing among views at every stage. We also presented extensive insights on transformer-based decoding schemes for 3D reconstruction and showed the advantages of the reconstruction via attention-based tensor decomposition on synthetic and real dataset.

Finally, several limitations of this work should be considered in the future. The output scheme has been explored



only for the occupancy grids. While in theory, it can be extended to signed distance fields with minimal changes. Furthermore, the performance was measured regarding the output resolution  $32^3$ . The method can be adapted to higher resolutions by only changing the output dimensionality or by integrating implicit refinement network like [7].

## 6. Acknowledgements

We thank Diego Martin Arroyo and Janis Postels for the discussions. We are also grateful to Google University Relationship GCP Credit Program for the support of this work by providing computational resources.

## References

- [1] Joshua Ainslie, Santiago Ontanón, Chris Alberti, Vaclav Cvicek, Zachary Fisher, Philip Pham, Anirudh Ravula, Sumit Sanghai, Qifan Wang, and Li Yang. Etc: Encoding long and structured inputs in transformers. *arXiv preprint arXiv:2004.08483*, 2020. 4
- [2] Gedas Bertasius, Heng Wang, and Lorenzo Torresani. Is space-time attention all you need for video understanding? *arXiv preprint arXiv:2102.05095*, 2021. 2
- [3] Alexey I Boyko, Mikhail P Matrosov, Ivan V Oseledets, Dzmitry Tsetserukou, and Gonzalo Ferrer. Tt-tsdf: Memory-efficient tsdf with low-rank tensor train decomposition. In *2020 IEEE/RSJ International Conference on Intelligent Robots and Systems (IROS)*, pages 10116–10121. IEEE, 2020. 2
- [4] Nicolas Carion, Francisco Massa, Gabriel Synnaeve, Nicolas Usunier, Alexander Kirillov, and Sergey Zagoruyko. End-to-end object detection with transformers. In *European Conference on Computer Vision*, pages 213–229. Springer, 2020. 2, 3
- [5] Angel X Chang, Thomas Funkhouser, Leonidas Guibas, Pat Hanrahan, Qixing Huang, Zimo Li, Silvio Savarese, Manolis Savva, Shuran Song, Hao Su, et al. Shapenet: An information-rich 3d model repository. *arXiv preprint arXiv:1512.03012*, 2015. 2, 6, 11, 12, 14
- [6] Zhiqin Chen and Hao Zhang. Learning implicit fields for generative shape modeling. In *Proceedings of the IEEE/CVF Conference on Computer Vision and Pattern Recognition*, pages 5939–5948, 2019. 12, 13
- [7] Julian Chibane, Thiemo Alldieck, and Gerard Pons-Moll. Implicit functions in feature space for 3d shape reconstruction and completion. In *IEEE Conference on Computer Vision and Pattern Recognition (CVPR)*. IEEE, jun 2020. 9
- [8] Christopher B Choy, Danfei Xu, JunYoung Gwak, Kevin Chen, and Silvio Savarese. 3d-r2n2: A unified approach for single and multi-view 3d object reconstruction. In *European conference on computer vision*, pages 628–644. Springer, 2016. 1, 2, 4, 5, 12, 13
- [9] Jia Deng, Wei Dong, Richard Socher, Li-Jia Li, Kai Li, and Li Fei-Fei. Imagenet: A large-scale hierarchical image database. In *2009 IEEE conference on computer vision and pattern recognition*, pages 248–255. Ieee, 2009. 3
- [10] Alexey Dosovitskiy, Lucas Beyer, Alexander Kolesnikov, Dirk Weissenborn, Xiaohua Zhai, Thomas Unterthiner, Mostafa Dehghani, Matthias Minderer, Georg Heigold, Sylvain Gelly, et al. An image is worth 16x16 words: Transformers for image recognition at scale. *arXiv preprint arXiv:2010.11929*, 2020. 2
- [11] John Duchi, Elad Hazan, and Yoram Singer. Adaptive sub-gradient methods for online learning and stochastic optimization. *Journal of machine learning research*, 12(7), 2011. 4
- [12] et al. Falcon, WA. Pytorch lightning. *GitHub. Note: https://github.com/PyTorchLightning/pytorch-lightning*, 3, 2019. 4
- [13] Jorge Fuentes-Pacheco, José Ruiz-Ascencio, and Juan Manuel Rendón-Mancha. Visual simultaneous localization and mapping: a survey. *Artificial intelligence review*, 43(1):55–81, 2015. 1, 2
- [14] Ben Graham, Alaaeldin El-Nouby, Hugo Touvron, Pierre Stock, Armand Joulin, Hervé Jégou, and Matthijs Douze. Levit: a vision transformer in convnet’s clothing for faster inference. *arXiv preprint arXiv:2104.01136*, 2021. 2
- [15] Thibault Groueix, Matthew Fisher, Vladimir G Kim, Bryan C Russell, and Mathieu Aubry. A papier-mâché approach to learning 3d surface generation. In *Proceedings of the IEEE conference on computer vision and pattern recognition*, pages 216–224, 2018. 12, 13
- [16] Richard A Harshman et al. Foundations of the parafac procedure: Models and conditions for an “explanatory” multi-modal factor analysis. 1970. 2
- [17] Kaiming He, Georgia Gkioxari, Piotr Dollár, and Ross Girshick. Mask r-cnn. In *Proceedings of the IEEE international conference on computer vision*, pages 2961–2969, 2017. 14
- [18] Mark W Jones. Distance field compression. 2004. 2
- [19] Abhishek Kar, Christian Häne, and Jitendra Malik. Learning a multi-view stereo machine. *arXiv preprint arXiv:1708.05375*, 2017. 1, 2
- [20] Arno Knapitsch, Jaesik Park, Qian-Yi Zhou, and Vladlen Koltun. Tanks and temples: Benchmarking large-scale scene reconstruction. *ACM Transactions on Graphics (ToG)*, 36(4):1–13, 2017. 4
- [21] Yehuda Koren, Robert Bell, and Chris Volinsky. Matrix factorization techniques for recommender systems. *Computer*, 42(8):30–37, 2009. 3
- [22] Zhenzhong Lan, Mingda Chen, Sebastian Goodman, Kevin Gimpel, Piyush Sharma, and Radu Soricut. Albert: A lite bert for self-supervised learning of language representations. *arXiv preprint arXiv:1909.11942*, 2019. 11
- [23] Joseph Levin. Three-mode factor analysis. *Psychological Bulletin*, 64(6):442, 1965. 2
- [24] Tsung-Yi Lin, Michael Maire, Serge Belongie, James Hays, Pietro Perona, Deva Ramanan, Piotr Dollár, and C Lawrence Zitnick. Microsoft coco: Common objects in context. In *European conference on computer vision*, pages 740–755. Springer, 2014. 14
- [25] Liyuan Liu, Xiaodong Liu, Jianfeng Gao, Weizhu Chen, and Jiawei Han. Understanding the difficulty of training transformers. *arXiv preprint arXiv:2004.08249*, 2020. 11

- [26] Lars Mescheder, Michael Oechsle, Michael Niemeyer, Sebastian Nowozin, and Andreas Geiger. Occupancy networks: Learning 3d reconstruction in function space. In *Proceedings of the IEEE/CVF Conference on Computer Vision and Pattern Recognition*, pages 4460–4470, 2019. [12](#), [13](#)
- [27] Pauli Miettinen and Stefan Neumann. Recent developments in boolean matrix factorization. *arXiv preprint arXiv:2012.03127*, 2020. [3](#)
- [28] Toan Q Nguyen and Julian Salazar. Transformers without tears: Improving the normalization of self-attention. *arXiv preprint arXiv:1910.05895*, 2019. [3](#)
- [29] Matthias Nießner, Michael Zollhöfer, Shahram Izadi, and Marc Stamminger. Real-time 3d reconstruction at scale using voxel hashing. *ACM Transactions on Graphics (ToG)*, 32(6):1–11, 2013. [2](#)
- [30] Onur Ozyesil, Vladislav Voroninski, Ronen Basri, and Amit Singer. A survey of structure from motion. *arXiv preprint arXiv:1701.08493*, 2017. [1](#), [2](#)
- [31] Niki Parmar, Ashish Vaswani, Jakob Uszkoreit, Lukasz Kaiser, Noam Shazeer, Alexander Ku, and Dustin Tran. Image transformer. In *International Conference on Machine Learning*, pages 4055–4064. PMLR, 2018. [3](#)
- [32] Stephan R Richter and Stefan Roth. Matryoshka networks: Predicting 3d geometry via nested shape layers. In *Proceedings of the IEEE conference on computer vision and pattern recognition*, pages 1936–1944, 2018. [12](#), [13](#)
- [33] Tammo Rukat, Chris C Holmes, and Christopher Yau. Tensor-machine: probabilistic boolean tensor decomposition. *arXiv preprint arXiv:1805.04582*, 2018. [2](#)
- [34] Karen Simonyan and Andrew Zisserman. Very deep convolutional networks for large-scale image recognition. *arXiv preprint arXiv:1409.1556*, 2014. [3](#)
- [35] Riccardo Spezialetti, David Joseph Tan, Alessio Tonioni, Keisuke Tateno, and Federico Tombari. A divide et impera approach for 3d shape reconstruction from multiple views. *arXiv preprint arXiv:2011.08534*, 2020. [2](#)
- [36] Xingyuan Sun, Jiajun Wu, Xiuming Zhang, Zhoutong Zhang, Chengkai Zhang, Tianfan Xue, Joshua B Tenenbaum, and William T Freeman. Pix3d: Dataset and methods for single-image 3d shape modeling. In *Proceedings of the IEEE Conference on Computer Vision and Pattern Recognition*, pages 2974–2983, 2018. [2](#), [6](#), [11](#), [14](#), [15](#), [16](#)
- [37] Maxim Tatarchenko, Alexey Dosovitskiy, and Thomas Brox. Octree generating networks: Efficient convolutional architectures for high-resolution 3d outputs. In *Proceedings of the IEEE International Conference on Computer Vision*, pages 2088–2096, 2017. [12](#), [13](#)
- [38] Maxim Tatarchenko, Stephan R Richter, René Ranftl, Zhuwen Li, Vladlen Koltun, and Thomas Brox. What do single-view 3d reconstruction networks learn? In *Proceedings of the IEEE/CVF Conference on Computer Vision and Pattern Recognition*, pages 3405–3414, 2019. [4](#)
- [39] Ledyard R Tucker. Some mathematical notes on three-mode factor analysis. *Psychometrika*, 31(3):279–311, 1966. [2](#)
- [40] Ashish Vaswani, Noam Shazeer, Niki Parmar, Jakob Uszkoreit, Llion Jones, Aidan N Gomez, Lukasz Kaiser, and Illia Polosukhin. Attention is all you need. *arXiv preprint arXiv:1706.03762*, 2017. [1](#), [2](#), [4](#)
- [41] Changlin Wan, Wennan Chang, Tong Zhao, Sha Cao, and Chi Zhang. Geometric all-way boolean tensor decomposition. *arXiv preprint arXiv:2007.15821*, 2020. [2](#)
- [42] Dan Wang, Xinrui Cui, Xun Chen, Zhengxia Zou, Tianyang Shi, Septimiu Salcudean, Z Jane Wang, and Rabab Ward. Multi-view 3d reconstruction with transformers. In *Proceedings of the IEEE/CVF International Conference on Computer Vision*, pages 5722–5731, 2021. [2](#), [5](#), [6](#)
- [43] Nanyang Wang, Yinda Zhang, Zhuwen Li, Yanwei Fu, Wei Liu, and Yu-Gang Jiang. Pixel2mesh: Generating 3d mesh models from single rgb images. In *Proceedings of the European Conference on Computer Vision (ECCV)*, pages 52–67, 2018. [12](#), [13](#)
- [44] Zhirong Wu, Shuran Song, Aditya Khosla, Fisher Yu, Linguang Zhang, Xiaoou Tang, and Jianxiong Xiao. 3d shapenets: A deep representation for volumetric shapes. In *Proceedings of the IEEE conference on computer vision and pattern recognition*, pages 1912–1920, 2015. [4](#)
- [45] Haozhe Xie, Hongxun Yao, Xiaoshuai Sun, Shangchen Zhou, and Shengping Zhang. Pix2vox: Context-aware 3d reconstruction from single and multi-view images. In *Proceedings of the IEEE/CVF International Conference on Computer Vision*, pages 2690–2698, 2019. [1](#), [2](#), [4](#), [5](#), [12](#), [13](#)
- [46] Haozhe Xie, Hongxun Yao, Shengping Zhang, Shangchen Zhou, and Wenxiu Sun. Pix2vox++: multi-scale context-aware 3d object reconstruction from single and multiple images. *International Journal of Computer Vision*, 128(12):2919–2935, 2020. [1](#), [2](#), [3](#), [4](#), [5](#), [12](#), [13](#), [14](#)
- [47] Bo Yang, Sen Wang, Andrew Markham, and Niki Trigoni. Robust attentional aggregation of deep feature sets for multi-view 3d reconstruction. *International Journal of Computer Vision*, 128(1):53–73, 2020. [5](#), [13](#)
- [48] Ming Zeng, Fukai Zhao, Jiaxiang Zheng, and Xinguo Liu. Octree-based fusion for realtime 3d reconstruction. *Graphical Models*, 75(3):126–136, 2013. [2](#)

# Supplementary Material

In this supplementary material we report additional experiments performed on ShapeNet [5]: ablation studies on hyper parameters of our model in Sec. A, an extended evaluation of LegoFormer for single view reconstruction broken down by category in Sec. B and more results comparing the different explored decoding schema in Sec. C. We also show more generalization results on the challenging Pix3D [36] dataset in Sec. D and extensively discuss limitations of the method in Sec. E.

## A. Additional ablation tests

We report here additional ablation studies to highlight the effect of different hyperparameters on the performance of the proposed architectures.

### A.1. Number of Decomposition Factors

In LegoFormer, the output volume is formed as a sum of  $n$  rank-1 approximations obtained by independently processing  $n$  learned queries. The number of approximations considered is correlated to the reconstruction performance achievable. Tab. 4 lists the performance of models trained with a different number of output queries against a different number of input views considered at test time. For each query count, the model was trained from scratch. As it can be easily observed, increasing the number of queries corresponds to an increase in performance—however, however the increase stalls after 12 queries. Interestingly, with only 2 queries a good IoU and F1-score performance can be achieved, only around 5 points lower than the best configurations. This means that our architecture can approximate very complex object shapes using as few as two rank-1 approximations.

### A.2. Training with different view counts

We also study the effect of the number of input views considered during training the LegoFormer-M model. We considered both using a fixed view count (2, 4 or 8) as well as random sampling the number of input views considered at every training iteration. Tab. 5 reports the results of these experiments. First of all, we can notice how, for the fixed number of inputs, there is a loose correlation between the number of training views and the performance at test time. Indeed, a model trained with few inputs performs better when running inference on few views and vice versa. This can be observed comparing the performance of the model trained with 4 and 8 views, the former outperforms the latter for any inference views count lower than 4, but after this threshold, the latter model performs better. By training with a dynamic number of views, we tried to achieve higher performance regardless of view count during the evaluation.

Views	Query count						
	2	3	4	6	8	12	16
<b>Metric: IoU</b>							
1	0.585	0.598	0.606	0.609	0.611	<b>0.617</b>	0.614
2	0.627	0.648	0.656	0.663	0.668	<b>0.674</b>	<b>0.674</b>
3	0.637	0.661	0.669	0.679	0.684	<b>0.689</b>	<b>0.689</b>
4	0.643	0.667	0.675	0.685	0.690	<b>0.695</b>	<b>0.695</b>
5	0.646	0.670	0.679	0.689	0.694	<b>0.699</b>	<b>0.699</b>
8	0.650	0.675	0.684	0.694	0.700	<b>0.704</b>	<b>0.704</b>
12	0.652	0.677	0.685	0.697	0.702	0.706	<b>0.707</b>
16	0.653	0.678	0.687	0.698	0.703	0.707	<b>0.708</b>
20	0.653	0.679	0.687	0.699	0.704	0.708	<b>0.709</b>
<b>Metric: F-score @ 1%</b>							
1	0.323	0.336	0.345	0.355	0.358	<b>0.364</b>	0.362
2	0.362	0.383	0.392	0.407	0.413	<b>0.422</b>	0.421
3	0.373	0.397	0.407	0.424	0.429	<b>0.438</b>	<b>0.438</b>
4	0.379	0.402	0.413	0.430	0.436	<b>0.445</b>	0.444
5	0.382	0.406	0.417	0.434	0.441	<b>0.449</b>	<b>0.449</b>
8	0.386	0.411	0.422	0.440	0.447	<b>0.455</b>	<b>0.455</b>
12	0.389	0.414	0.424	0.443	0.451	0.457	<b>0.458</b>
16	0.389	0.415	0.425	0.445	0.452	<b>0.459</b>	<b>0.459</b>
20	0.390	0.415	0.426	0.445	0.453	0.459	<b>0.461</b>

Table 4. Comparison of the reconstruction performance with respect to the number of queries used on the decoder side. For each number of queries a separate model was trained from scratch.

Unfortunately, we observed harder convergence with this setup resulting in lower performance. This could be linked to the instability problems of the transformer training [25]. We plan to investigate further this aspect of the model in future works.

### A.3. Reducing model dimensionality

The parameter count of the transformer models can grow pretty quickly, resulting in higher memory requirements. A number of techniques were proposed to counteract the parameter growth of transformer architectures. One of the techniques is to share weights between transformer encoder and decoder layers, as proposed in ALBERT [22]. Using this technique, only a single transformer layer is defined for the encoder and decoder, and the layer is repeatedly applied to the input. We experiment with this technique and were able to reduce the model size by 5.5 times, from 168M to 30.6M parameters, while experiencing minor performance drop as reported in Tab. 6. Based on this experiment, we show that there exist a nice trade-off between memory requirement and performance for LegoFormer architectures, and the former can be decreased significantly without affecting the latter much.

Training view count	Evaluation view count								
	1	2	3	4	5	8	12	16	20
<b>Metric: IoU</b>									
2	0.635	0.668	0.677	0.681	0.684	0.688	0.690	0.691	0.691
4	0.617	0.674	0.689	0.695	0.699	0.704	0.706	0.707	0.708
8	0.519	0.644	0.679	0.694	0.703	0.713	<b>0.717</b>	<b>0.719</b>	<b>0.721</b>
[1, 10)	0.601	0.638	0.652	0.659	0.663	0.669	0.672	0.673	0.674
Pix2Vox++/A [46]	<b>0.670</b>	<b>0.695</b>	<b>0.704</b>	<b>0.708</b>	<b>0.711</b>	<b>0.715</b>	<b>0.717</b>	0.718	0.719
<b>Metric: F-score @ 1%</b>									
2	0.377	0.412	0.421	0.426	0.428	0.433	0.435	0.436	0.437
4	0.364	0.422	0.438	0.445	0.449	0.455	0.457	0.459	0.459
8	0.282	0.392	0.428	0.444	0.453	<b>0.464</b>	<b>0.470</b>	<b>0.472</b>	<b>0.473</b>
[1, 10)	0.349	0.384	0.398	0.404	0.409	0.415	0.418	0.419	0.420
Pix2Vox++/A [46]	<b>0.436</b>	<b>0.452</b>	<b>0.455</b>	<b>0.457</b>	<b>0.458</b>	0.459	0.460	0.461	0.462

Table 5. Effect of the number of input views used during training on the inference-time performance on the ShapeNet dataset at  $32^3$  resolution. In the setup of the column [1, 10) view count is changed at every iteration to a number between 1 and 9, inclusive. We also report the performance of the strongest competitor, Pix2Vox++/A [46] as a reference.

Setup View Count	IoU			F-Score@1%		
	Vanilla	Parameter Sharing	Difference	Vanilla	Parameter Sharing	Difference
1 view	<b>0.617</b>	0.596	-0.021	<b>0.364</b>	0.345	-0.019
2 views	<b>0.674</b>	0.661	-0.013	<b>0.422</b>	0.406	-0.016
3 views	<b>0.689</b>	0.678	-0.011	<b>0.438</b>	0.424	-0.014
4 views	<b>0.695</b>	0.685	-0.010	<b>0.445</b>	0.432	-0.013
5 views	<b>0.699</b>	0.691	-0.008	<b>0.449</b>	0.438	-0.011
8 views	<b>0.704</b>	0.697	-0.007	<b>0.455</b>	0.444	-0.011
12 views	<b>0.706</b>	0.700	-0.006	<b>0.457</b>	0.448	-0.009
16 views	<b>0.707</b>	0.701	-0.006	<b>0.459</b>	0.449	-0.010
20 views	<b>0.708</b>	0.702	-0.006	<b>0.459</b>	0.450	-0.009

Table 6. Comparison between a vanilla LegoFormer and a parameter sharing LegoFormer on the ShapeNet dataset. In the latter case, all layers of the encoder and decoder use the same parameters, meaning that a single layer is repeatedly applied for each side resulting in using  $5.5\times$  less parameters.

## B. Single view performance per category

We extend the single view evaluation of LegoFormer on ShapeNet [5] in Tab. 7 where we compare it against 10 recent state-of-the-art methods that predict voxel grids [8, 32, 37, 45, 46], triangle meshes [15, 43] or implicit representations [6, 26]. We report both category-wise performance and "overall", i.e., the average over the available classes for each method. In almost every category, LegoFormer-S shows competitive performance against the other methods. Also, LegoFormer-S performs significantly better than LegoFormer-M in all categories, showing the importance of using attention-based encoding. Overall, the

proposed method is competitive with recent proposals in the literature, outperforming several of them.

## C. Comparison to other decoding schemes - Qualitative Results

In Fig. 8 we show some qualitative examples of reconstructions using the different decoding schemes discussed in Section 3.2 of the main paper. In contrast to the naive approaches where the voxels are independently predicted, LegoFormer outputs are more structured and do not contain spike-like spurious full voxels (e.g., the small artifacts on the bottom right corner of the lamp reconstructed by



Method															
Category		3D-R2N2	OGN [37]	Matryoshka	AtlasNet [15]	Pix2Mesh	OccNet [26]	IM-Net [6]	AttSets [47]	Pix2Vox/F	Pix2Vox/A	Pix2Vox++	Pix2Vox++	LegoForm	LegoForm
IoU															
airplane		0.513	0.587	0.647	0.493	0.508	0.532	<b>0.702</b>	0.594	0.600	0.684	0.607	0.674	0.480	0.641
bench		0.421	0.481	0.577	0.431	0.379	0.597	0.564	0.552	0.538	<b>0.616</b>	0.544	0.608	0.326	0.612
cabinet		0.716	0.729	0.776	0.257	0.732	0.674	0.680	0.783	0.765	0.792	0.782	<b>0.799</b>	0.640	0.780
car		0.798	0.828	0.850	0.282	0.670	0.671	0.756	0.844	0.837	0.854	0.841	<b>0.858</b>	0.724	0.852
chair		0.466	0.483	0.547	0.328	0.484	0.583	<b>0.644</b>	0.559	0.535	0.567	0.548	0.581	0.442	0.557
display		0.468	0.502	0.532	0.457	0.582	<b>0.651</b>	0.585	0.565	0.511	0.537	0.529	0.548	0.391	0.524
lamp		0.381	0.398	0.408	0.261	0.399	<b>0.474</b>	0.433	0.445	0.435	0.443	0.448	0.457	0.428	0.453
speaker		0.662	0.637	0.701	0.296	0.672	0.655	0.683	0.721	0.707	0.714	0.721	<b>0.721</b>	0.645	0.712
rifle		0.544	0.593	0.616	0.573	0.468	0.656	<b>0.723</b>	0.601	0.598	0.615	0.594	0.617	0.465	0.632
sofa		0.628	0.646	0.681	0.354	0.622	0.669	0.694	0.703	0.687	0.709	0.696	<b>0.725</b>	0.483	0.707
table		0.513	0.536	0.573	0.301	0.536	<b>0.659</b>	0.621	0.590	0.587	0.601	0.609	0.620	0.489	0.596
telephone		0.661	0.702	0.756	0.543	0.762	0.794	0.762	0.743	0.77	0.776	0.782	<b>0.809</b>	0.569	0.787
watercraft		0.513	0.632	0.591	0.355	0.471	0.579	0.607	0.601	0.582	0.594	0.583	0.603	0.467	<b>0.608</b>
overall		0.560	0.596	0.635	0.352	0.552	0.626	0.659	0.642	0.634	0.661	0.645	<b>0.670</b>	0.519	0.655
F-Score@1%															
airplane		0.412	0.487	0.446	0.415	0.376	0.494	<b>0.598</b>	0.489	-	-	0.493	0.583	0.349	0.501
bench		0.345	0.364	0.424	0.439	0.313	0.318	0.361	0.406	-	-	0.399	<b>0.478</b>	0.229	0.459
cabinet		0.327	0.316	0.381	0.350	<b>0.450</b>	0.449	0.345	0.367	-	-	0.363	0.408	0.254	0.391
car		0.481	0.514	0.481	0.319	0.486	0.315	0.304	0.497	-	-	0.523	<b>0.564</b>	0.364	0.525
chair		0.238	0.226	0.302	0.406	0.386	0.365	<b>0.442</b>	0.334	-	-	0.262	0.309	0.193	0.269
display		0.227	0.215	0.400	0.451	0.319	<b>0.468</b>	0.466	0.310	-	-	0.253	0.296	0.187	0.274
lamp		0.267	0.249	0.276	0.217	0.219	0.361	<b>0.371</b>	0.315	-	-	0.287	0.315	0.289	0.307
speaker		0.231	0.225	<b>0.279</b>	0.199	0.190	0.249	0.200	0.211	-	-	0.256	0.152	0.218	0.278
rifle		0.521	0.541	0.514	0.405	0.340	0.219	0.407	0.524	-	-	0.553	<b>0.574</b>	0.417	0.563
sofa		0.274	0.290	0.326	0.337	0.343	0.324	0.354	0.334	-	-	0.320	<b>0.377</b>	0.192	0.367
table		0.340	0.352	0.374	0.373	0.502	<b>0.549</b>	0.461	0.419	-	-	0.385	0.406	0.276	0.369
telephone		0.504	0.528	0.598	0.545	0.485	0.273	0.423	0.469	-	-	0.588	<b>0.633</b>	0.355	0.572
watercraft		0.305	0.328	0.360	0.296	0.266	0.347	0.369	0.315	-	-	0.346	<b>0.390</b>	0.274	0.386
overall		0.351	0.368	0.391	0.362	0.398	0.393	0.405	0.395	-	-	0.394	<b>0.436</b>	0.282	0.404

Table 7. Comparison of single-view reconstruction between models on ShapeNet at 32<sup>3</sup> resolution. Mean IoU and F-Score@1% reported for all categories.

Naive-Full). This observation supports our claim that using a tensor decomposition-based parametrization acts like a regularization and constrains the output space. The second row in the figure, is a relatively hard case for all approaches due to the unusual positioning of the armrests on the bench. While no model correctly reconstructs the 3D shape, all predictions are significantly noisier than the one obtained by LegoFormer-M. The same can be said of the reconstructed sofa in the first row, where all alternatives struggle to generate nice flat surfaces except for LegoFormer-M.

## D. Reconstruction consistency on real-world data

We report in Fig. 9 additional predictions on Pix3D [36] obtained by a LegoFormer-S model. Besides the full predicted voxel grids, we report also the individual outputs predicted by the decoder for each query incrementally aggregated together. This is similar to what we show in Fig. 7 of the main paper for LegoFormer-M. To ease the visualization of the individual part decomposition for this experiment we trained a variant of LegoFormer-S on ShapeNet [5] with only 6 output queries instead of the 12 used in the main paper.

The results confirms what highlighted for LegoFormer-M in the main paper: the queries tend to specialize into different type of 3D structures, with the first 4 mainly predicting flat horizontal planes and the last two focusing more on vertical surfaces like the chair and table legs (second to the last) or the backrest of the chair. These results also show some limitations in the generalization performance of LegoFormer-S when applied to real data. For example the chair backrest is not properly reconstructed, likely because the color of the chair does not have much contrast with the white background and the network fails to detect it. We will discuss more about limitations in the following section.

## E. Limitations

We show here some limitations of LegoFormer-S when applied to the challenging real data from Pix3D [36]. For all the following results we use LegoFormer-S trained on the ShapeNet [5] dataset and tested without fine tuning it on the real images. This setting is particularly challenging due to the domain gap existing between real and synthetic data and helps to highlight failures of the network. During our experiments we identified several sources of "failure":

**Unseen Categories.** In Fig. 10 we show four examples of failed reconstructions of objects outside the categories available in the training set. The first three images represent *close* out-of-distribution samples belonging to the *bed* category which is not present in ShapeNet but it is relatively similar to other furniture categories. For this reason the network generates a 3D model that resembles a mix between

a sofa and an arm chair, two of the available categories in the training set. While wrong in terms of overall shape and proportions, the predictions do try to capture some of the characteristics of the images, like the elongated shape of the bed in the second column. The last column shows a far out-of-distribution sample belonging to the *bowl* category. There isn't a similar category in the ShapeNet training data and for this reason the model fails generating a meaningless output. We believe that these limitations could be alleviated by training on a more varied synthetic dataset to enlarge the set of categories considered in-distribution.

**Occlusions.** While ShapeNet [5] always depicts objects perfectly visible and without any kind of occlusions, this is not true for the real data. For this reason the model might generate wrong predictions in such cases. We report some of these examples in Fig. 11. In the first column the network is probably confused by the presence of objects on the table surface and reconstructs the table as a chair. In this case occlusions cause a non uniform "texture" of the object, all ShapeNet [5] models have instead uniform textures, however sofas and armchairs can exhibit non uniform colors due to shading effects. The second column shows an example of partial occlusions since the arms of the chair are occluded by the man sitting on it. In this case the network reconstructs only the clearly visible part of the object resulting in an arm-less chair. Finally the third and fourth columns show additional examples where distracting elements (the pillows) and occlusions makes once again the model fail badly (third column) or be mislead on the proportion of the object (fourth column). We believe that this weakness could be partially overcome by simulating occlusions during training, which we are not currently doing. Moreover we show here results for the single-view model, but part of these failures could maybe be overcome in the presence of multiple views, where the occluded parts should change from view to view.

**Failed tensor decomposition.** In Fig. 12 we show three examples where our proposed tensor decomposition fails to generate some details of the real models. For example the legs of the chairs and the bottom part of the table are missing or broken in the reconstruction. As any other compression method a rank-1 decomposition can have the side effect of removing details. We believe that part of the missing details, if needed, could be recovered from the raw output of LegoFormer pre-thresholding with an additional small refiner network similar to what done in [46].

**Bad Segmentation Mask.** All the results so far have used the GT segmentation masks to segment out the object from the background, in Fig. 13 we show the impact on performance of using predicted masks from a Mask-RCNN model [17] trained on COCO [24]. As expected non perfect masks lead to a degradation on the quality of the predicted models. Fine-tuning the Mask-RCNN model on the

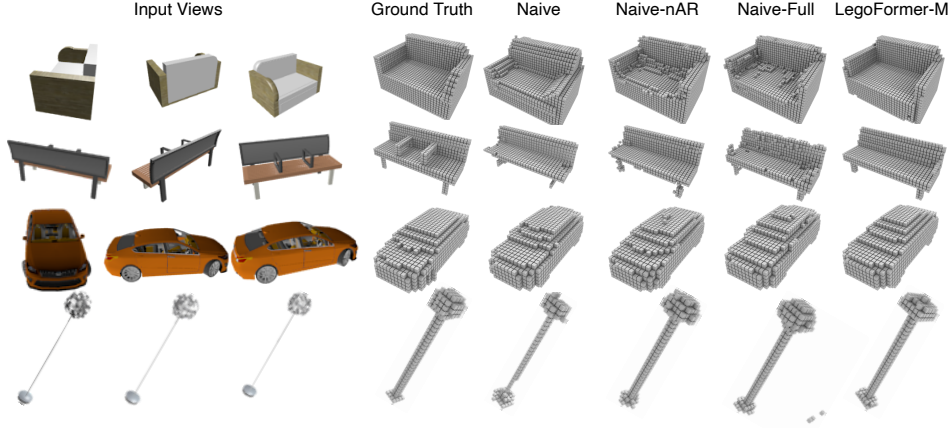


Figure 8. Multi-view object reconstructions of the four decoding schemes for 3 input views on ShapeNet with  $32^3$  resolution. The second row shows an example of a challenging case for all decoding schemes.

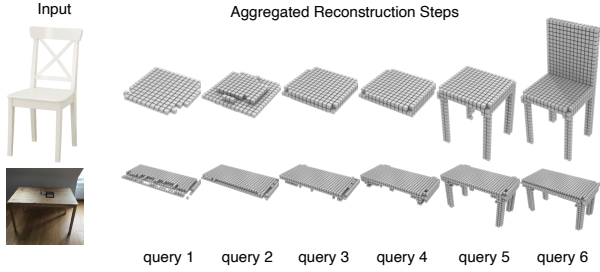


Figure 9. Incremental reconstruction on the Pix3D [36] dataset. For this experiment we used a LegoFormer-S trained using 6 decomposition queries to ease the visualization.



Figure 10. Failed reconstructions of LegoFormer-S on data from Pix3D [36]. We selected four challenging out-of-distribution samples as they belong to the *bed* and *bowl* categories which are not present in the training set. While for the beds the model tries to come up with predictions which are a mix of a sofa and an arm-chair (the two most related classes in the training set), for the bowl the model fails completely.

desired categories can certainly help to alleviate these issues by improving the segmentation performance. Another option could be to train our model using synthetic rendering placed in front of random background. If this training

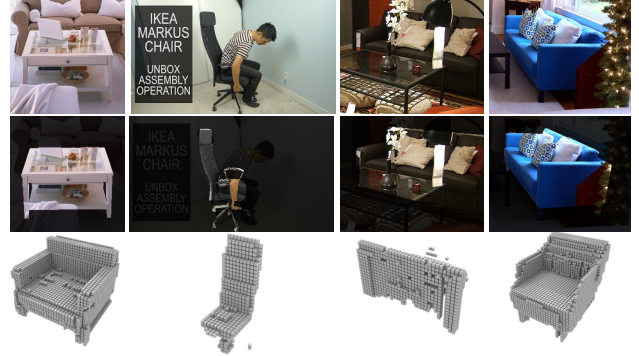


Figure 11. Failed reconstructions of LegoFormer-S on data from Pix3D [36] in presence of occlusions. The first row shows the original image, the second row the image segmented according to the GT object segmentation mask (the input to LegoFormer-S), finally the last row show the 3D model predicted. Due to occlusions our model is mislead into predicting objects from different categories (column one), can generate only partial shape (column two) or fails the reconstruction altogether due to too much clutter (column three) or misleading perspective (column four).

succeeds we could potentially drop the dependency from a nicely segmented input altogether.



Figure 12. Failure cases for LegoFormer-S on Pix3D [36] data due to failed rank-1 tensor decomposition for the output grid. The model fails to predict tiny structures like the chair and table legs.

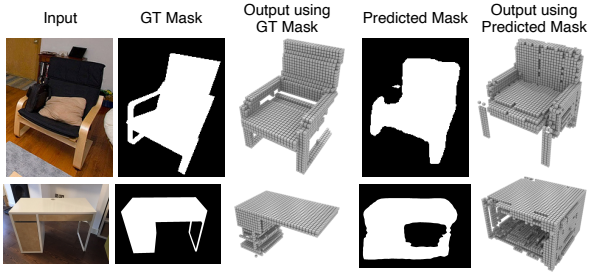


Figure 13. Model reconstructed by a LegoFormer-S model on Pix3D [36] using GT masks to segment the object from the background (third column) or predicted masks (last column). The use of non-optimal masks lead to a clear degradation in performance.